A lung-inspired printed circuit board polymer electrolyte fuel cell

V. S. Bethapudi [a,b], J. Hack [b], P. Trogadas [a], J. I. S. Cho [a], L. Rasha [b], G. Hinds [c], P. R. Shearing [b], D. J. L. Brett [b,*] and M.-O. Coppens [a, **]

[a] EPSRC "Frontier Engineering" Centre for Nature Inspired Engineering & Department of Chemical Engineering, University College London, London WC1E 7JE, United Kingdom

[b] Electrochemical Innovation Lab, Department of Chemical Engineering, University College London, London WC1E 7JE, United Kingdom

[c] National Physical Laboratory, Hampton Road, Teddington, Middlesex TW11 0LW, United Kingdom

Abstract

Fractal cathode flow-fields, inspired by the flow mechanism of air inside lungs, can provide homogeneous, scalable and uniform distribution of reactants to polymer electrolyte fuel cell (PEFC) electrodes. However, the complex 3D flow-fields demonstrated previously face manufacturing challenges, such as requiring selective laser sintering, an additive manufacturing method that is expensive to scale up. Here, a lung-inspired cathode flow-field is introduced and fabricated using low-cost, lightweight printed circuit boards (PCB). The uniformity and alignment between individual PCB layers producing the fractal hierarchy of flow channels have been characterised using X-ray computed tomography (X-ray CT). The performance of the fractal flow-field exceeds that of conventional single-serpentine flow-fields and is particularly beneficial when operating on air with a low relative humidity. The lung-inspired design is shown to lead to a more stable operation than the single-serpentine design, as a result of uniform distribution of reactants.

Keywords: Fractal flow-field; X-ray computed tomography; polarisation; printed circuit board; lung-inspired.

* Corresponding author.
d.brett@ucl.ac.uk
Professor of Electrochemical Engineering
Department of Chemical Engineering
University College London
Torrington Place
London, WC1E 7JE
+44 (0) 20 7679 3310
** Corresponding author.
m.coppens@ucl.ac.uk
Ramsay Memorial Professor & Head of Department of Chemical Engineering
Director, EPSRC "Frontier Engineering" Centre for Nature Inspired Engineering (CNIE)
Department of Chemical Engineering
University College London
Torrington Place
London, WC1E 7JE
+44 (0) 20 7679 7369 (internal 37369)

1. Introduction

Polymer electrolyte fuel cells (PEFCs) operating on hydrogen are considered to be an ideal replacement for a wide range of power sources for many stationary, portable, built environment and transport applications, due to their low temperature operation, zero emissions at point of use, high efficiency, high power density, and rapid start-up [1–3].

Flow-field plates are important components for PEFCs; they provide the necessary mechanical compression to hold individual components together and they introduce oxidant (air) and fuel (hydrogen) to the respective electrodes [4,5]. A wide range of flow-fields have been developed, incorporating serpentine, parallel, interdigitated, pin, mesh, cascade, perforated and biomimetic designs [6–14]. A major operational issue that could be impacted by the structure of the flow-field is accumulation of water in the channels and under the land areas, especially at the cathode [6,15–17]. Water accumulation or flooding in the flow channels is commonly observed due to inefficient removal of liquid water by reactant gases. Flooding leads to non-uniform reactant distribution on the electrode surface, resulting in a heterogeneous current density distribution that can hinder performance and accelerate degradation [7,18,19].

Serpentine flow channels are widely acknowledged as having operational advantages in terms of uniform reactant distribution, water and heat management and effective utilisation of electrocatalysts [6,20–24] . However, their design needs to be improved to overcome issues such as: a decrease in fuel cell performance at low current density under low temperature and low relative humidity conditions [25]; a significant decrease in reactant concentration from inlet to outlet of the fuel cell [26]; uneven reactant consumption and current density distribution [27]; cathode water accumulation during higher humidity operation [15,28]; and high pressure drop at large scale (> 10 cm^2 area of the flow-field) [29].

Nature has evolved scalable, hierarchical architectures for fluid distribution that are highly effective and thermodynamically optimised, such respiratory organs, the vascular network and plants [30–33]. Some of these desirable flow mechanisms and fundamental principles observed in nature have been implemented in developing fuel cell flow-field structures. Through numerical modelling and simulation, Asadzade et al. [34] identified lung-shaped microfluidic flow patterns in bipolar plates as a means of maximising power density. Kloess et al. [8] established, via simulations and experimental studies, that serpentine and interdigitated flow-fields, when integrated with lung and leaf flow patterns, delivered enhanced performance. Guo et al. [10] mimicked the hierarchical structures of leaf veins, with three hierarchical generations, by incorporating them into serpentine and interdigitated flow-fields, leading to improved performance over conventional flow-fields. Arvay et al. [9] reviewed CFD simulations applied to nature-inspired flow-fields and concluded that the efficacy of these designs increases when used in conjunction with standard interdigitated designs. Collectively, these studies show that decreased pressure drop, uniform flow distribution, higher oxygen delivery and homogeneous reactant distribution can all be achieved by using nature-inspired designs.

Coppens [35,36] developed a systematic and thematic nature-inspired chemical engineering (NICE) methodology that leverages fundamental mechanisms underpinning desirable properties in natural systems, such as scalability, efficiency and robustness, in designs that address similar challenges in engineering, for a range of applications. NICE designs adopt the natural mechanisms, but adapt them to the different context of the technological application, recognising that nature and technology operate under different constraints [36]. Applied to fuel cell design, Kjelstrup, Coppens et al. [37] proposed a lung-inspired, conceptual design for the fractal gas distribution system and the catalytic layers of fuel cells that results in minimum entropy generation and enhanced performance. Work by Marquis [38] and Trogadas, Cho et al. [29] applied the NICE approach to the analysis of lung-inspired, fractal flow-fields. Initial modelling and simulation studies were performed to optimise the distributor structure and identify the optimal number of fractal branching generations to achieve uniform reactant distribution. Further, laser sintering of stainless steel was used to construct the 3D flow-field structure, and it was found that, up to four generations, the fractal flow-field exhibited significant performance enhancement over conventional flow-field designs. However, this study [29] identified difficulties in water management at higher humidity that resulted in performance degradation for higher numbers of generations. Furthermore, the weight (approximately 0.5 kg per flow-field), complexity, time and cost (£600-£800 per flow-field) involved in the flow-field fabrication (laser sintering of stainless steel) can hinder the use of fractal structures in commercial fuel cells and stacks. In summary, while the benefits of a NICE approach to flow-field design are clear, a common concern is the cost and manufacturability of these complex 3D structures at scale.

Incorporating the membrane electrode assembly (MEA) within the layers of printed circuit boards (PCBs) has proven to be a promising means of PEFC fabrication due to the ease of manufacturability, durability and adaptability, as well as the light weight and cost effectiveness [39–44]. However, to date the PCB flow-fields have conformed to conventional ‘2D’ flow configurations. In this study, we combine the cost effective PCB approach with a hierarchical lung-inspired flow-field design for the first time. A 3D fractal flow-field is constructed using a 2D planar multi-layered PCB approach. The performance of the lung-inspired flow-field is measured in an operating PEFC over a range of relative humidities and compared with that of a conventional, single-serpentine flow-field.

2. Experimental

2.1 Lung-inspired flow-field design

Hierarchically structured 3D lung-inspired flow-field plates were constructed using a 2D planar layer-wise approach, as shown in Fig. 1 (a); “a” is a PCB plate coated with 38 μm of copper, which adjoins the membrane electrode assembly (MEA).

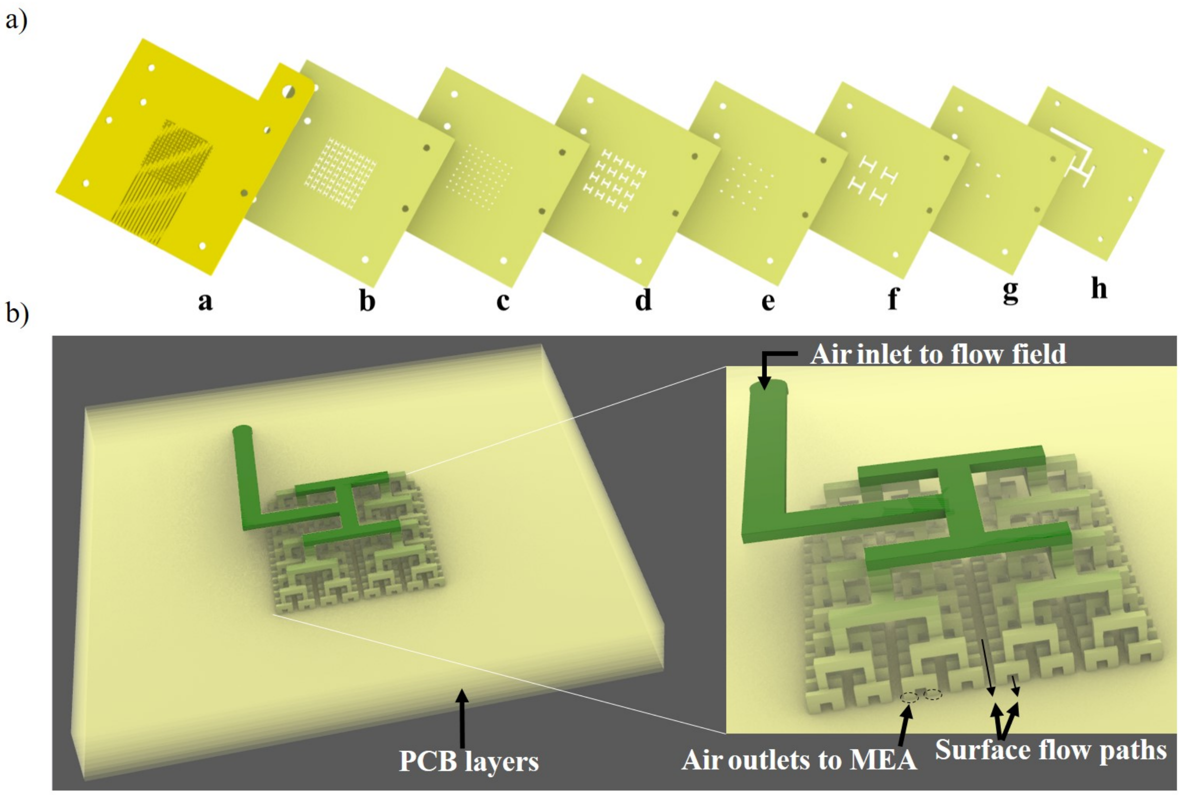

Fig. 1: (a) PCB plates a-h comprising 2D planar individual layers of hierarchical fractal flow-field geometry. (b) RHINO model depicting the assembly of individual PCB layers, resulting in a fractal flow-field geometry. Shown are the single air inlet, multiple air outlets to MEA level, and the surface flow paths for the cathode air and water outlets from the fuel cell.

Each of the plates “a-h” corresponds to a specific generation within the fractal geometry. Fig. 1 (b) shows the four generations of fractal flow, with airflow from a single inlet to 256 outlets (end of the 4th generation) at the interface with the MEA. The total MEA active area covered by these outlets is 6.25 cm^2.

Each of the 4th generation outlets has a dimension of 400 μm × 800 μm with 1.18 mm spacing between adjacent outlets. Surface flow paths (0.5 mm wide and 1 mm deep) between these outlets are used for the removal of cathode air and excess water within the fuel cell (a previous study adopted a dead-ended removal mechanism [29]).

2.2 Flow-field fabrication

A Roland-40 CNC machine (ROLAND, USA) was used to cut the channel features for each layer. The fabricated individual plates are shown in supplementary data Fig. S1 (a). Plate “a” was electroplated with Ni, followed by Au, and acted as the cathode current collector. The Ni plating solution was 0.13 M $Ni(SO_3NH_2)_2$ and the Au plating solution was 0.02 M $KAu(CN)_2$. Plate “a” (1.6 mm in thickness) was electroplated with Ni at a constant current density of 4.3 mA cm^{-2} (corresponding to an applied voltage of 3.0 V - 3.5 V) for 3 min, followed by electroplating with Au at a constant current density of 2.4 mA cm^{-2} (corresponding to an applied voltage of 3.0 V - 3.7 V) for 60 min. Plates “b-h” were uncoated plain PCB plates.

Plates “a-h” were then assembled in a hot press at 140 °C under 400 psig compression for 1 hour. Layers of prepreg thermosetting polymer sheets acted as an adhesive between the PCB plates. The final assembled cathode fractal flow-field plate, having an overall thickness of 9.6 mm, with dimensions as shown in Fig. S1 (supplementary data).

The anode flow-field plate contained a single serpentine flow channel, with a width, spacing and depth of 1 mm each and it also functioned as the anode current collector. It was fabricated from a PCB plate of thickness similar to plate “a”. Ni and Au layers were electrodeposited on the anode flow-field plate as described above for plate “a”. The final assembled anode flow-field plate, similar in dimensions to the fractal flow-field plate but having an overall thickness of 3.5 mm, is shown in supplementary data Fig. S1 (b). This anode flow-field was used for PEFC testing with both the cathode fractal flow-field and the cathode single-serpentine flow-field.

The cathode single-serpentine flow-field, which also acted as the cathode current collector, was similar in design, material, dimensions and fabrication method to the anode flow-field plate (process as above, including Ni and Au coating). However, the flow outlet from the cathode flow-field was from the surface via vertical channels of 0.5 mm width and 1 mm depth and with a spacing of 1.18 mm between adjacent channels, as shown in supplementary data Fig. S2.

2.3 MEA preparation

The MEA (active area 6.25 cm^2) was prepared by hot pressing of a Nafion 212® (DuPont, USA) membrane and HyPlat Pt catalyst (HyPlat, South Africa) coated gas diffusion electrodes at 150 °C for 3 min under an applied pressure of 400 psig. Both electrodes had a catalyst loading of 0.4 mg Pt cm^{-2}. The Gas Diffusion Layer (GDL) used was Freudenberg H23C9, which is a carbon fibre paper with a total thickness of 210 μm, including a PTFE treated microporous layer (MPL). The overall thickness of the MEA after hot pressing was ~500 μm.

2.4 Fuel cell assembly

The overall fuel cell assembly and the individual components involved in testing the fuel cells are shown in Fig. 2. The MEA was assembled between a pair of Tygaflor gaskets having a thickness of 250 μm each. The cell was heated at start up to 45 °C using cylindrical 75 W heating cartridges of 6.5 mm × 60 mm in dimensions (RS Components, UK).

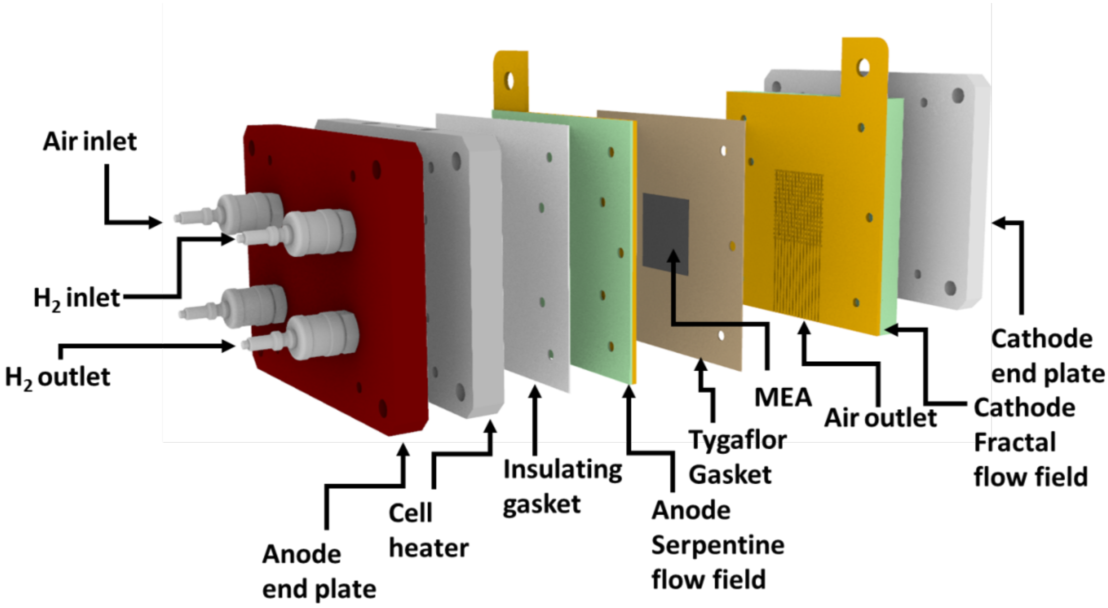

Fig. 2: PEFC components and assembly diagram.

A self-adhesive K-type thermocouple (OMEGA, UK) was attached to the anode flow-field to measure the cell surface temperature (due to the difference in plate thickness between the cathode single-serpentine and cathode lung-inspired flow-fields, the anode region is preferred). An insulating gasket was provided between the heating plate and flow-field plate to avoid electrical short-circuiting within the cell. Aluminium end-plates were used to provide overall compression to the assembly, with a torque of 1.2 Nm provided to the bolts running through them. Air inlet, hydrogen inlet and hydrogen outlet were provided from the manifolds on the anode end-plate, while air outlet was provided from the surface of the cathode flow-field, as shown in Fig. 2. The fuel cells were operated under ambient cooling, and no additional cooling channels or devices were present.

2.5 X-Ray Computed Tomography (X-ray CT)

An X-ray CT scan was performed on the lung-inspired flow-field plate using a Nikon 225 XT (Nikon Metrology, UK). The experimental setup for the scan is shown in Fig. 3 (a).

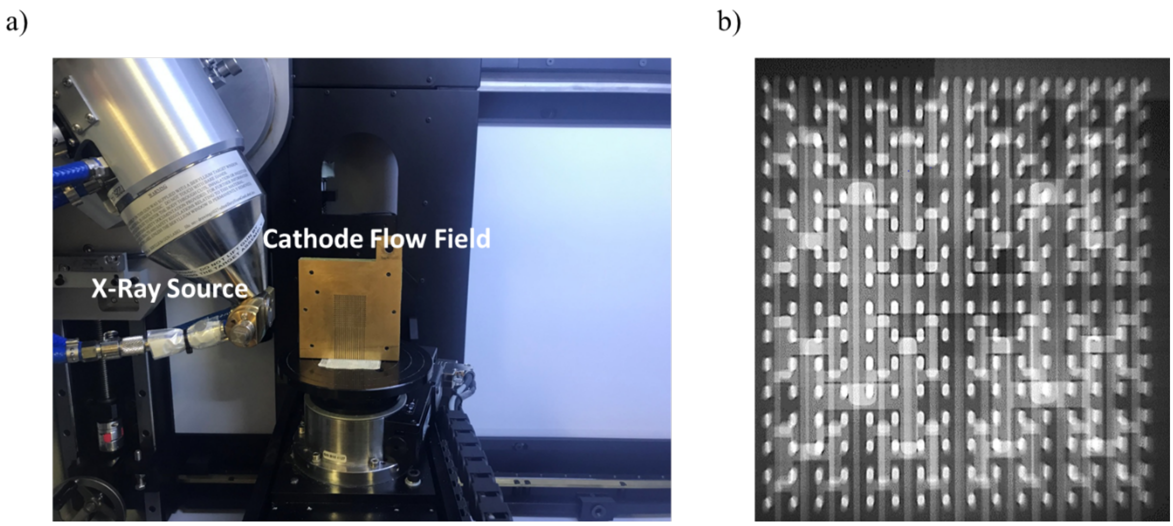

Fig. 3: (a) Experimental setup for X-ray CT scanning, (b) radiograph of the region of interest (ROI) of the scanned lung-inspired flow-field.

The scan was performed using a beam voltage of 170 kV, a beam current of 240 μA and a scan rate of 1 frame per second. The region of interest (ROI) was chosen to be the lung-inspired flow-field (Fig. 3 (b)), with a sample distance from the detector selected to ensure the entire flow-field remained within the field-of-view (FOV) through the 360° of scanning (Fig. 3 (a)). The total acquisition time was 53 min with collection of 3176 radiographs. A filtered back projection (FBP) reconstruction algorithm (using

Nikon CT Pro 3D software – a built in software with Nikon 225 XT) was applied to the images to result in a three-dimensional dataset with a voxel size of 17 µm. Image analysis was done using Avizo (Thermo-Fischer Scientific, USA), by importing the dataset into the software and analysing individual orthoslices in the three planes (xz, yz and xy).

2.6 Fuel cell testing

The fuel cell testing was carried out using a Scribner 850e fuel cell test station (Scribner Associates NC, USA). The test station had the capability to supply reactants at desired conditions, using temperature, humidity and mass flow controllers. The test station provided hydrogen at 99.995% purity under ambient temperature conditions. Hydrogen flow was maintained at 100 mL min^{-1} throughout, while the cathode airflow stoichiometry was 3.0 [45]. The fuel cell was tested at three different cathode and anode relative humidity (RH) levels: 40%, 70% and 100%.

Electrochemical impedance spectroscopy (EIS) measurements were carried out using a Gamry Reference 3000 and Gamry Reference 30k Booster (Gamry Instruments, USA). The frequency range for analysis was 0.1 Hz to 100 kHz, with 10 points per decade, and an AC modulation amplitude of 5% of the DC input signal.

3. Results and Discussion

3.1 X-ray CT scan analysis

An X-ray CT scan of the lung-inspired flow-field, as shown in Fig. 4, visualises the internal channel arrangement of the flow-field and the alignment of individual layers, as well as the quality of the cell assembly. Fig.4 (a) shows a volume rendering of the region scanned. This is a 3D representation of the entire sample; a video tracking slice by slice through the 3D lung-inspired flow-field can be accessed by clicking Fig. 4. Fig. 4 (b) shows a virtual slice in the yz plane, displaying four fractal generations. The layers are clearly visible and there is good alignment between layers of the PCB without any overlap of channels. The dark grey regions, where the attenuation is lower, correspond to the flow channels (voids) in the fractal geometry. In addition, Fig. 4 (c) shows the virtual slice of the 3rd generation fractal outlets from the front face, i.e. showing the entire flow-field. This further highlights that the outlet channels are unobscured with no misalignment.

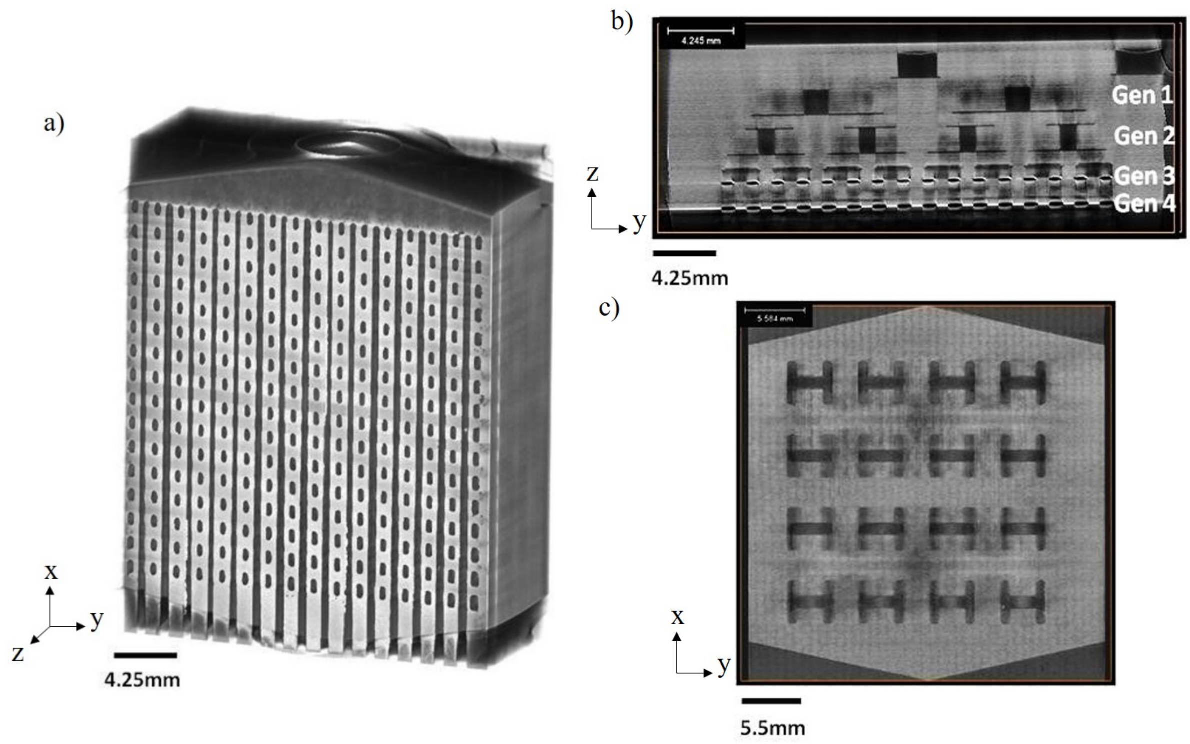

Fig. 4: (a) Volume rendering of the scanned area of the lung-inspired flow-field and 3D track through video, (b) virtual slice in the yz plane showing the hierarchical fractal flow structure with four generations and (c) virtual slice in the xy plane showing the layout of channels at the 3rd generation outlets.

3.2 PEFC performance

Polarisation curves were measured between open-circuit voltage (OCV) and 0.3 V, where each data point was recorded at 0.05 V intervals with 30s hold [46] at each interval. Measurements were carried out at three different RH levels - 40% RH, 70% RH and 100% RH - for the single-serpentine and lung-inspired cathode flow-fields, as shown in Fig. 5.

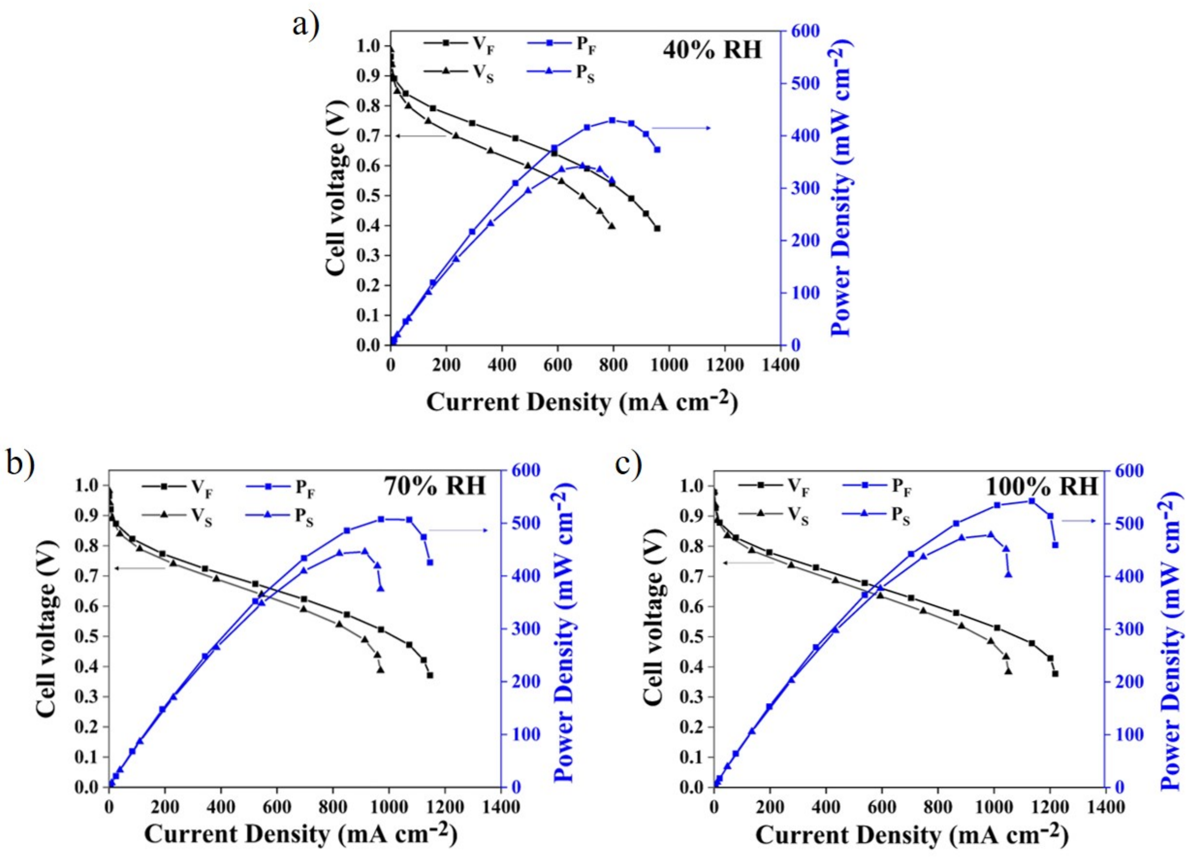

Fig. 5: Polarisation curves at (a) 40% RH, (b) 70% RH and (c) 100% RH. (Legend: V_F – cell voltage with fractal flow-field; V_S – cell voltage with serpentine flow-field; P_F – power density with fractal flow-field; V_S – power density with serpentine flow-field).

The lung-inspired fuel cell shows better performance compared to the single-serpentine fuel cell under all conditions. The optimal performance current density, which was measured at 0.6 V [47] cell voltage and taken to be a trade-off between efficiency and power, at 40% RH, 70% RH and 100% RH with the single-serpentine cathode flow-field was: 510 mA cm^{-2}, 680 mA cm^{-2} and 700 mA cm^{-2}, respectively; with the lung-inspired flow-field it was appreciably higher, namely, 705 mA cm^{-2}, 760 mA cm^{-2} and 800 mA cm^{-2}, respectively. This corresponds to an increase in performance of 41%, 12% and 14% of the lung-inspired design over the single-serpentine fuel cell, at 40% RH, 70% RH and 100% RH, respectively.

The higher performance of the lung-inspired flow-field is attributed to its fractal geometry, with equal hydraulic path lengths between the inlet and all the outlets. This results in a transition from convective to diffusive air flow at the outlets, which distributes the reactants uniformly over the surface of the MEA [29]. The difference in performance between the lung-inspired and single-serpentine flow-fields decreases with increasing RH, particularly in the activation and ohmic regions, which is attributed to the improved conductivity of the membrane [48,49]. It is likely that the higher velocity of air in the serpentine flow-field channels leads to excessive drying of the membrane at low RH, leading to reduced membrane conductivity and cell performance. However, the performance of the lung-inspired design in the mass transport limited regime is much better compared to the single-serpentine flow-field, irrespective of reactant RH.

It is clear that the lung-inspired flow-field performs better than the conventional serpentine flow-field at higher current density and is less subject to mass transport issues, such as water flooding and reactant starvation [50,51]. Furthermore, the presence of vertical flow paths, as shown in Fig. 1 and Fig. S 1(a), results in more effective water management compared to the previous dead-ended design [29], which flooded during operation at higher RH [29]. Severe mass transport limitations are evident in the cell with a single-serpentine flow-field compared to a lung-inspired flow-field at higher current density, between 900 mA cm^{-2} and 1100 mA cm^{-2}, where its performance reduces drastically [52], as seen in Figs. 5 (b) and 5 (c).

3.3 Temperature measurements

The increase in cell temperature while measuring the polarisation curves was monitored, as shown in Fig. 6. At higher current density, there are mass transport limitations, and the cell temperature has a significant influence on the degree of liquid water saturation. Lower cell temperatures result in higher water retention at MEA level and a corresponding decrease in current density, and *vice versa* [53,54]. From Fig. 6 it can be observed that, at a given current density, higher cell temperatures are developed in the single-serpentine flow-field at low reactant RH (40%), which can be attributed to membrane dehydration, while lower cell temperatures for the single-serpentine flow-field (despite operating at lower potentials compared to the lung-inspired flow-field) are developed at improved reactant RH (70% and 100%), which can be attributed to the occurrence of flooding in the cell.

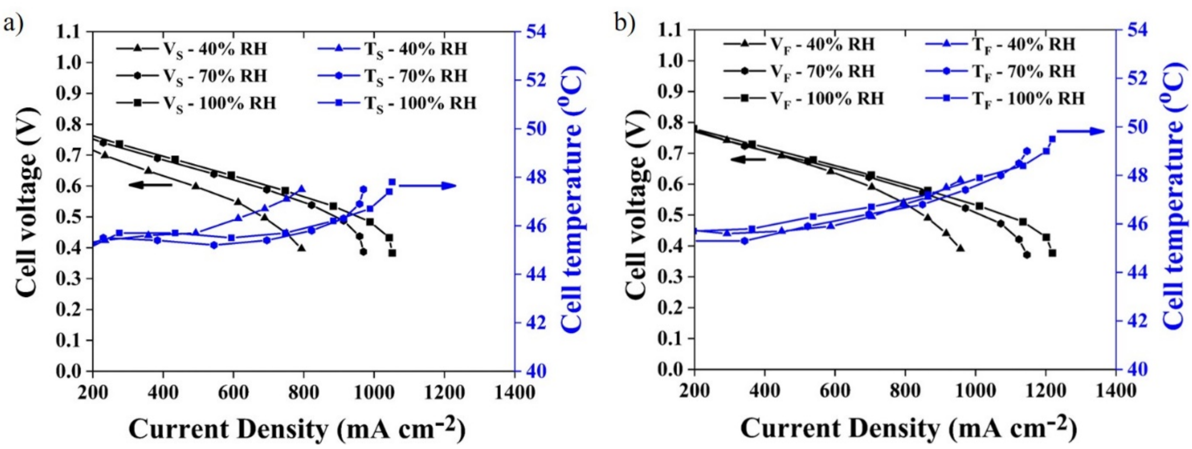

Fig. 6: Cell temperature during polarisation curve measurements for (a) single-serpentine flow-field and (b) lung-inspired flow-field at 40% RH, 70% RH and 100% RH. (Legend: V_S – cell voltage with serpentine flow-field; V_F – cell voltage with fractal flow-field; T_S – serpentine flow-field temperature; T_F – fractal flow-field temperature).

Further, it can be observed that the increase in cell temperature for the single-serpentine flow-field is initially slow and later rises rapidly beyond 500 mA cm^{-2} at 40% RH and beyond 800 mA cm^{-2} for 70% RH and 100% RH, whereas for the lung-inspired design it increases much more gradually throughout the accessible current density range. This may be due to more uniform hydration of the MEA arising from the use of the lung-inspired flow-field, compared to that using the single-serpentine flow-field, where a non-uniform temperature increase is caused by the presence of localised dry and flooded regions. Apart from flooding, membrane resistance plays a crucial role in fuel cell performance, especially at low RH, and, hence, its effect is demonstrated in the next section.

Overall, the lung-inspired flow-field allows higher operating temperatures that result in superior performance compared to the single-serpentine flow-field.

3.4 Impedance measurements

EIS was performed between 0.1 Hz and 100 kHz for the single-serpentine and lung-inspired flow-fields over a range of current densities [55,56]. To obtain a stable measurement, the cells were held at the respective current density and reactant conditions constantly for 2 min before the corresponding EIS was performed. The EIS spectra at 300 mA cm^{-2}, 600 mA cm^{-2} and 900 mA cm^{-2} are shown in Figs. 7 (a), (b) and (c).

At the lowest current density of 300 mA cm^{-2}, the charge transfer resistance observed for the lung-inspired and single-serpentine cells is almost identical, under all humidity conditions tested (corresponding equivalent circuit and charge transfer values are given in supplementary data Fig. S3 and Table S1, respectively). Increasing the current density to 600 mA cm^{-2}, the charge transfer and mass transport resistances

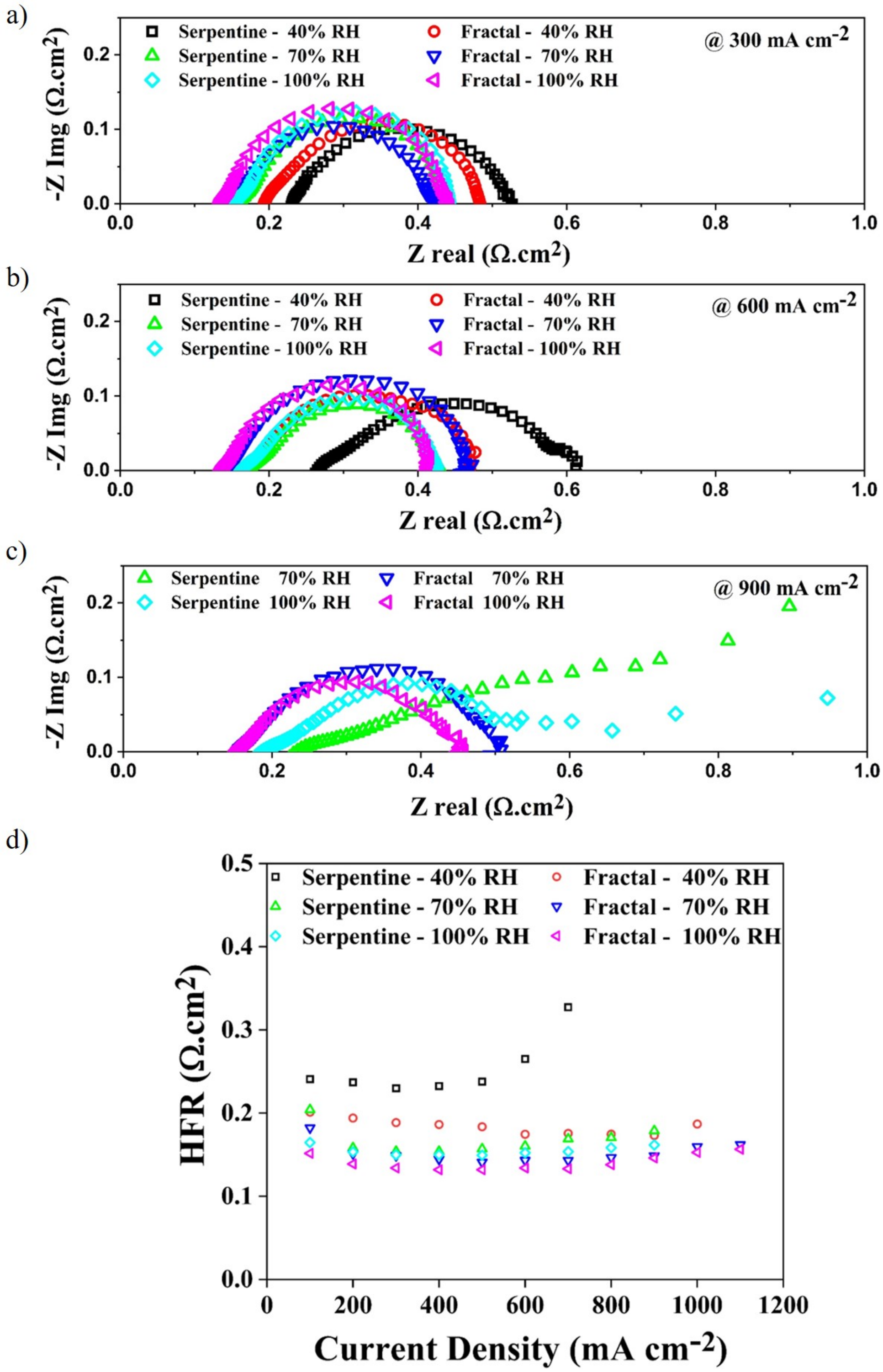

Fig. 7: Electrochemical impedance spectra for single-serpentine and fractal flow-fields at (a) 300 mA cm^{-2}, (b) 600 mA cm^{-2} and (c) 900 mA cm^{-2}, at 40% RH, 70% RH and 100% RH. (d) HFR for single-serpentine and lung-inspired flow-fields at 40% RH, 70% RH and 100% RH.

(R_{mt}) (equivalent circuit is depicted in Fig. S3 [57]) for the cell with lung-inspired flow-field (R_{mt} is 0.025 $\Omega.cm^2$ and 0.03 $\Omega.cm^2$ at 70% RH and 100% RH, respectively) are lower than those with the single-serpentine flow-field (R_{mt} is 0.042 $\Omega.cm^2$ and 0.044 $\Omega.cm^2$ at 70% RH and 100% RH, respectively). Finally, at 900 mA cm^{-2}, the cell with the single-serpentine flow-field has significantly higher charge transfer and mass transfer resistances (R_{mt} is 0.16 $\Omega.cm^2$ and 0.9 $\Omega.cm^2$ at 70% RH and 100% RH, respectively) compared to the lung-inspired flow-field (R_{mt} is 0.03 $\Omega.cm^2$ and 0.04 $\Omega.cm^2$ at 70% RH and 100% RH, respectively), implying that it is subject to excessive flow channel flooding that results in much lower levels of oxygen concentration at the cathode [58].

In contrast, the cell with the lung-inspired flow-field shows a well-defined, stable and lower charge transport resistance with minimal or no mass transport/diffusive impedance. This demonstrates the ability of the lung-inspired design to distribute reactant gases and water uniformly over the MEA surface, maintaining a well-hydrated system, clear of any flooding in the flow path under a wider range of operating conditions. This is consistent with the improved performance in the mass transport region of the cell with the lung-inspired flow-field, as seen in Fig. 5.

The high frequency resistance (HFR), which is determined from the high-frequency intercept with the real axis of the Nyquist plots (obtained from the EIS measurements as outlined in section 2.6) in Fig. 7, provides a measure of the ohmic resistance and is predominantly attributed to the membrane hydration and its associated conductivity [59,60]. Fig. 7 (d) shows that at 70% RH and 100% RH the membrane resistance initially decreases, as water is produced in the electrochemical reaction, goes through a minimum, and then increases as the cell temperature increases, leading to membrane dehydration. This is well established behaviour [61] and common to both flow-field designs.

The generally higher resistance at low RH (40%) indicates a less uniformly hydrated membrane. Even so, the resistance of the cell with the lung-inspired flow-field design remains relatively stable over the operational range, while that with the serpentine flow-field is significantly higher and increases rapidly for current densities above 500 mA cm^{-2}. This steep increase can be attributed to severe reduction in membrane conductivity due to membrane dehydration [41,62,63]. This suggests that the superior performance of the lung-inspired flow-field system at low RH can be attributed to the diffusion dominated, uniformly distributed and low velocity reactant flow occurring through the fractal structure [32,64] that minimises membrane dehydration while enabling higher temperature operation (Fig. 6(b)).

3.5 Operating stability

A galvanostatic test was performed to evaluate performance stability of the PEFC under both relatively dry and relatively humid conditions. Fig. 8 shows galvanostatic measurements at 40% RH (dry) and 70% RH (humid) conditions, where the current density is maintained at 700 mA cm^{-2} and 750 mA cm^{-2}, respectively. At 40% RH, the performance of the lung-inspired flow-field is more stable compared to that of the single-serpentine flow-field over the entire duration of the test; the cell voltage variation for the lung-inspired and single-serpentine flow-fields ranged within 4% and 8%, respectively, of their initial values. Furthermore, at 70% RH the cell voltage variation range for the lung-inspired flow-field decreases to 2%, while for single-serpentine it is much higher at 12%.

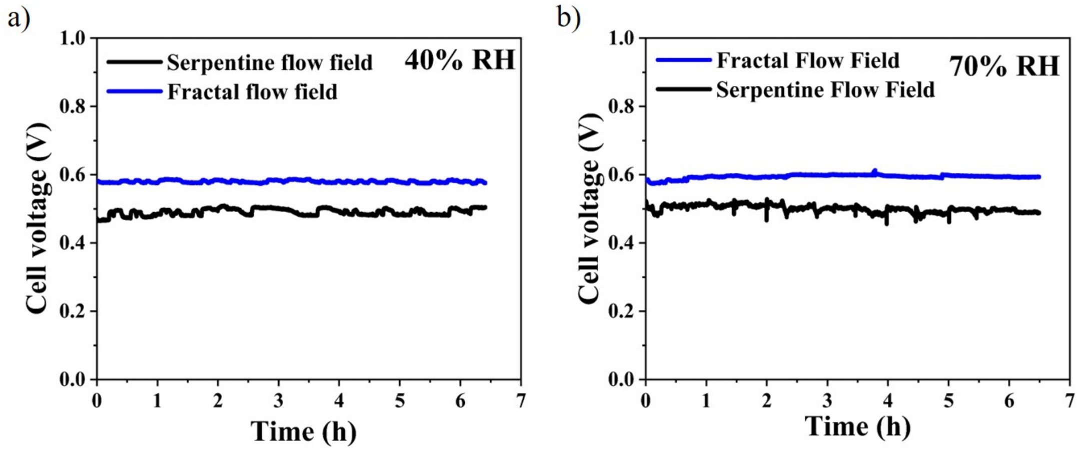

Fig. 8: Cell voltage fluctuation over 6 h during galvanostatic tests at (a) 40% RH and 700 mA cm^{-2} and (b) 70% RH and 750 mA cm^{-2}.

Cell voltage fluctuations and erratic behaviour are related to liquid water accumulation in the gas distribution channels and its uneven removal [65,66]. Increase in water accumulation decreases the voltage, and *vice versa* [67]. The results in Fig. 8 provide further evidence of a more uniform water distribution and cell performance in the lung-inspired design, compared to the conventional single-serpentine design. The convection dominated gas flow in the single-serpentine flow-field may have resulted in uneven levels of water saturation, creating regions of high and low water retention (flooding and drying) [28]. In addition, the single-serpentine flow-field could be subject to periodic localised flooding [68], suggested by the cell voltage fluctuations [69,70]. In previous work, the extent of the cell voltage fluctuations (peaks in Fig. 8 (a) and 8 (b)) has been linked to the degree of flooding in a fuel cell [71], the degree of hydration of the membrane and its level of swelling [72]. Increasing RH from 40% to 70% increases the level of cell voltage fluctuations for the single-serpentine flow-field, indicative of greater flooding in channels at higher RH. However, the lung-inspired system remains stable when humidity increases, consistent with more uniformity in water distribution. This is in line with the improved transport of reactants via lung-inspired flow-fields.

4. Conclusions

This study is the first to combine a fractal, lung-inspired cathode flow-field with a low cost PCB- based manufacturing technique, via a layer-wise assembly approach. The PCB approach offers a cost-effective alternative to previously reported fabrication methods for such flow-fields, which employed selective laser sintering. This also opens up the possibility of easily scalable manufacturing of fractal flow structures for a range of other applications.

X-ray CT scans of the flow-field indicated well aligned and properly assembled PCB layers, confirming the precision of the adopted method of manufacturing. The lung-inspired flow-field delivered enhanced performance compared to a conventional single-serpentine flow-field. Polarisation curves indicated a performance enhancement in lung-inspired flow-fields by 41%, 12% and 14% at 0.6V cell potential for 40%, 70% and 100% reactant humidity (RH) conditions, respectively. Higher operating temperatures by 2-3 ºC were observed in the lung-inspired flow-field that resulted in its superior performance over the single-serpentine flow-field.

In addition, the performance enhancement in the lung-inspired flow-field was particularly observed at high RH and high current density. Electrochemical impedance spectroscopy was used to show that this is due to more uniform distribution of reactants and water management in the cell; the mass transfer resistances developed at 100% RH and higher current density (~900 mA cm^{-2}) were 0.04 $\Omega.cm^2$ for lung-inspired flow-field and 0.9 $\Omega.cm^2$ for single-serpentine flow-field. Galvanostatic tests on the flow-fields indicate a much more stable operation of lung-inspired PEFC;

voltage fluctuations at constant current hold for lung-inspired and single-serpentine were observed to be within 2% and 12% of their initial values at relatively humid reactant conditions.

Acknowledgements

The authors would like to acknowledge funding from the EPSRC "Frontier Engineering" Award (EP/K038656/1), the EPSRC (EP/L015277/1, EP/P009050/1, EP/M014371/1, EP/M009394/1, EP/M023508/1, EP/L015749/1, EP/N022971/1) for supporting fuel cell research in the Electrochemical Innovation Lab (EIL). We also thank the Department of Chemical Engineering, University College London, and the National Measurement System of the UK Department of Business, Energy and Industrial Strategy for supporting this work.

5. References

[1] T. Elmer, M. Worall, S. Wu, S.B. Riffat, Fuel cell technology for domestic built environment applications: State of-the-art review, Renew. Sustain. Energy Rev. 42 (2015) 913–931. doi:10.1016/j.rser.2014.10.080.

[2] T. Wilberforce, A. Alaswad, A. Palumbo, M. Dassisti, A.G. Olabi, Advances in stationary and portable fuel cell applications, Int. J. Hydrogen Energy. 41 (2016) 16509–16522. doi:10.1016/j.ijhydene.2016.02.057.

[3] A. Alaswad, A. Baroutaji, H. Achour, J. Carton, A. Al Makky, A.G. Olabi, Developments in fuel cell technologies in the transport sector, Int. J. Hydrogen Energy. 41 (2016) 16499–16508. doi:10.1016/j.ijhydene.2016.03.164.

[4] V. Mehta, J.S. Cooper, Review and analysis of PEM fuel cell design and manufacturing, J. Power Sources. 114 (2003) 32–53. doi:10.1016/S0378-7753(02)00542-6.

[5] X. Li, I. Sabir, Review of bipolar plates in PEM fuel cells: Flow-field designs, Int. J. Hydrogen Energy. 30 (2005) 359–371. doi:10.1016/j.ijhydene.2004.09.019.

[6] A.P. Manso, F.F. Marzo, J. Barranco, X. Garikano, M. Garmendia Mujika, Influence of geometric parameters of the flow fields on the performance of a PEM fuel cell. A review, Int. J. Hydrogen Energy. 37 (2012) 15256–15287. doi:10.1016/j.ijhydene.2012.07.076.

[7] J. Wang, Theory and practice of flow field designs for fuel cell scaling-up: A critical review, Appl. Energy. 157 (2015) 640–663. doi:10.1016/j.apenergy.2015.01.032.

[8] J.P. Kloess, X. Wang, J. Liu, Z. Shi, L. Guessous, Investigation of bio-inspired flow channel designs for bipolar plates in proton exchange membrane fuel cells, J. Power Sources. 188 (2009) 132–140. doi:10.1016/j.jpowsour.2008.11.123.

[9] A. Arvay, J. French, J.C. Wang, X.H. Peng, A.M. Kannan, Nature inspired flow field designs for proton exchange membrane fuel cell, Int. J. Hydrogen Energy. 38 (2013) 3717–3726. doi:10.1016/j.ijhydene.2012.12.149.

[10] N. Guo, M.C. Leu, U.O. Koylu, Bio-inspired flow field designs for polymer electrolyte membrane fuel cells, Int. J. Hydrogen Energy. 39 (2014) 21185–21195. doi:10.1016/j.ijhydene.2014.10.069.

[11] D.L. Wood, J.S. Yi, T. V Nguyen, Effect of direct liquid water injection and interdigitated flow field on the performance of proton exchange membrane fuel cells, Electrochim. Acta. 43 (1998) 3795-3809 .doi:10.1016/S0013-4686(98)00139-X.

[12] T. Van Nguyen, M.W. Knobbe, A liquid water management strategy for PEM fuel cell stacks, 114 (2003) 70–79. doi:10.1016/S0378-7753(02)00591-8.

[13] P.J. Hamilton, B.G. Pollet, Polymer electrolyte membrane fuel cell (PEMFC) flow field plate: Design, materials and characterisation, Fuel Cells. 10 (2010) 489–509. doi:10.1002/fuce.201000033.

[14] S. Subramaniam, G. Rajaram, K. Palaniswamy, Comparison of perforated and serpentine fl ow fi elds on the performance of proton exchange membrane fuel cell, J. Energy Inst. 90 (2017) 363–371. doi:10.1016/j.joei.2016.04.006.

[15] A. Iranzo, P. Boillat, J. Biesdorf, A. Salva, Investigation of the liquid water

distributions in a 50 cm 2 PEM fuel cell : Effects of reactants relative humidity , current density , and cathode stoichiometry, Energy. 82 (2015) 914–921. doi:10.1016/j.energy.2015.01.101.

[16] D. Spernjak, A.K. Prasad, S.G. Advani, Experimental investigation of liquid water formation and transport in a transparent single-serpentine PEM fuel cell, J. Power Sources , 170 (2007) 334–344. doi:10.1016/j.jpowsour.2007.04.020.

[17] J.P. Owejan, T.A. Trabold, D.L. Jacobson, D.R. Baker, D.S. Hussey, M. Arif, In situ investigation of water transport in an operating PEM fuel cell using neutron radiography : Part 2 – Transient water accumulation in an interdigitated cathode flow field, Int. J. Heat Mass Transf. 49 (2006) 4721–4731. doi:10.1016/j.ijheatmasstransfer.2006.07.004.

[18] Z. Wang, Y. Zeng, S. Sun, Z. Shao, B. Yi, Improvement of PEMFC water management by employing water transport plate as bipolar plate, Int. J. Hydrogen Energy. 42 (2017) 21922–21929. doi:10.1016/j.ijhydene.2017.07.052.

[19] W. Schmittinger, A. Vahidi, A review of the main parameters influencing long-term performance and durability of PEM fuel cells, J. Power Sources. 180 (2008) 1–14. doi:10.1016/j.jpowsour.2008.01.070.

[20] J.P. Feser, A.K. Prasad, S.G. Advani, On the relative influence of convection in serpentine flow fields of PEM fuel cells, J. Power Sources. 161 (2006) 404–412.doi:10.1016/j.jpowsour.2006.04.129.

[21] D.H. Jeon, S. Greenway, S.Ã. Shimpalee, J.W. Van Zee, The effect of serpentine flow-field designs on PEM fuel cell performance, Int. J. Hydrogen

Energy.33 (2008) 1052–1066.doi:10.1016/j.ijhydene.2007.11.015.

[22] X.D. Wang, Y.Y. Duan, W.M. Yan, Novel serpentine-baffle flow field design for proton exchange membrane fuel cells, J. Power Sources. 173 (2007) 210–221. doi:10.1016/j.jpowsour.2007.08.037.

[23] K.S. Choi, H.M. Kim, S.M. Moon, An experimental study on the enhancement of the water balance, electrochemical reaction and power density of the polymer electrolyte fuel cell by under-rib convection, Electrochem. Commun. 13 (2011) 1387–1390. doi:10.1016/j.elecom.2011.08.015.

[24] J.H. Nam, K.J. Lee, S. Sohn, C.J. Kim, Multi-pass serpentine flow-fields to enhance under-rib convection in polymer electrolyte membrane fuel cells: Design and geometrical characterization, J. Power Sources. 188 (2009) 14–23. doi:10.1016/j.jpowsour.2008.11.093.

[25] L. Wang, A. Husar, T. Zhou, H. Liu, A parametric study of PEM fuel cell performances, Int. J. Hydrogen Energy. 28 (2003) 1263–1272. doi:10.1016/S0360-3199(02)00284-7.

[26] X. Li, I. Sabir, J. Park, A flow channel design procedure for PEM fuel cells with effective water removal, J. Power Sources. 163 (2007) 933–942. doi:10.1016/j.jpowsour.2006.10.015.

[27] W. Sun, B.A. Peppley, K. Karan, Modeling the influence of GDL and flow-field plate parameters on the reaction distribution in the PEMFC cathode catalyst layer, J. Power Sources.144 (2005) 42–53. doi:10.1016/j.jpowsour.2004.11.035.

[28] K. Tüber, D. Pócza, C. Hebling, Visualization of water buildup in the cathode of

a transparent PEM fuel cell, J. Power Sources. 124 (2003) 403–414. doi:10.1016/S0378-7753(03)00797-3.

[29] P. Trogadas, J.I.S. Cho, T.P. Neville, J. Marquis, B. Wu, D.J.L. Brett, M.O. Coppens, A lung-inspired approach to scalable and robust fuel cell design, Energy Environ. Sci. 11 (2018) 136–143. doi:10.1039/c7ee02161e.

[30] F.C. Meinzer, M.J. Clearwater, G. Goldstein, Water transport in trees : current perspectives , new insights and some controversies, Environ. Exp. Bot. 45 (2001) 239–262. doi:10.1016/S0098-8472(01)00074-0

[31] Z. Smalko, An impact of thermodynamic processes in human bodies on performance reliability of individuals, J. Konbin. 27 (2015) 5–22. doi:10.2478/jok-2013-0101.

[32] S. Gheorghiu, S. Kjelstrup, P. Pfeifer3, M.-O. Coppens, Is the Lung an Optimal Gas S. Gheorghiu, S. Kjelstrup, P. Pfeifer and M.-O. Coppens, in Fractals in Biology and Medicine, ed. G. A. Losa, D. Merlini, T. F. Nonnenmacher and E. R. Weibel, Birkha¨user Basel, Basel, 2005, pp. 31–42. doi: 10.1007/3-7643-7412-8_3.

[33] P. Trogadas, M.M. Nigra, M.O. Coppens, Nature-inspired optimization of hierarchical porous media for catalytic and separation processes, New J. Chem. 40 (2016) 4016–4026. doi:10.1039/c5nj03406j.

[34] M. Asadzade, A. Shamloo, Design and simulation of a novel bipolar plate based on lung-shaped bio-inspired flow pattern for PEM fuel cell, Int. J. Energy Res. 41 (2017) 1730–1739.

[35] M.O. Coppens, Scaling-up and -down in a nature-inspired way, Ind. Eng.

Chem. Res. 44 (2005) 5011–5019. doi:10.1021/ie0490482.

[36] M.O. Coppens, A nature-inspired approach to reactor and catalysis engineering, Curr. Opin. Chem. Eng. 1 (2012) 281–289. doi:10.1016/j.coche.2012.03.002.

[37] S. Kjelstrup, M.O. Coppens, J.G. Pharoah, P. Pfeifer, Nature-inspired energy- and material-efficient design of a polymer electrolyte membrane fuel cell, Energy and Fuels. 24 (2010) 5097–5108. doi:10.1021/ef100610w.

[38] J. Marquis, PhD thesis, Rensselaer Polytechnic Institute, Troy, NY, 2013.

[39] R. O'Hayre, D. Braithwaite, W. Hermann, S.J. Lee, T. Fabian, S.W. Cha, Y. Saito, F.B. Prinz, Development of portable fuel cell arrays with printed-circuit technology, J. Power Sources. 124 (2003) 459–472. doi:10.1016/S0378-7753(03)00802-4.

[40] R. Lin, Y. Weng, X. Lin, F. Xiong, Rapid cold start of proton exchange membrane fuel cells by the printed circuit board technology, Int. J. Hydrogen Energy. 39 (2014) 18369–18378. doi:10.1016/j.ijhydene.2014.09.065.

[41] O.A. Obeisun, Q. Meyer, J. Robinson, C.W. Gibbs, A.R. Kucernak, P.R. Shearing, D.J.L. Brett, Development of open-cathode polymer electrolyte fuel cells using printed circuit board flow-field plates: Flow geometry characterisation, Int. J. Hydrogen Energy. 39 (2014) 18326–18336. doi:10.1016/j.ijhydene.2014.08.106.

[42] Y. Wu, J.I.S. Cho, T.P. Neville, Q. Meyer, R. Ziesche, P. Boillat, M. Cochet, P.R. Shearing, D.J.L. Brett, E ff ect of serpentine flow- field design on the water management of polymer electrolyte fuel cells : An in-operando neutron

radiography study, J. Power Sources. 399 (2018) 254–263 doi:10.1016/j.jpowsour.2018.07.085.

[43] J.I.S. Cho, T.P. Neville, P. Trogadas, J. Bailey, P. Shearing, D.J.L. Brett, M.O. Coppens, Capillaries for water management in polymer electrolyte membrane fuel cells, Int. J. Hydrogen Energy. 43 (2018) 21949–21958. doi:10.1016/j.ijhydene.2018.10.030.

[44] E. Engebretsen, J.B. Robinson, O. Obeisun, T. Mason, D. Finegan, G. Hinds, P.R. Shearing, D.J.L. Brett, Electro-thermal impedance spectroscopy applied to an open-cathode polymer electrolyte fuel cell, J. Power Sources. 302 (2016) 210–214. doi:10.1016/j.jpowsour.2015.10.047.

[45] A. Kazim, Exergy analysis of a PEM fuel cell at variable operating conditions, Energy Convers. Manag. 45 (2004) 1949–1961. doi:10.1016/j.enconman.2003.09.030.

[46] Q. Meyer, S. Ashton, P. Boillat, M. Cochet, E. Engebretsen, D.P. Finegan, X. Lu, J.J. Bailey, N. Mansor, R. Abdulaziz, O.O. Taiwo, R. Jervis, S. Torija, P. Benson, S. Foster, P. Adcock, P.R. Shearing, D.J.L. Brett, Effect of gas diffusion layer properties on water distribution across air-cooled , open-cathode polymer electrolyte fuel cells : A combined ex- situ X-ray tomography and in-operando neutron imaging study, Electrochim. Acta. 211 (2016) 478–487. doi:10.1016/j.electacta.2016.06.068.

[47] U.S. Department of Energy, Fuel Cells Section, Multi-Year Res. Dev. Demonstr. Plan. 2015 (2015) 1–58.

[48] Y. Sone, Proton Conductivity of Nafion 117 as Measured by a Four-Electrode

AC Impedance Method, J. Electrochem. Soc. 143 (1996) 1254. doi:10.1149/1.1836625.

[49] H. Al-Zeyoudi, A.P. Sasmito, T. Shamim, Performance evaluation of an open-cathode PEM fuel cell stack under ambient conditions: Case study of United Arab Emirates, Energy Convers. Manag. 105 (2015) 798–809. doi:10.1016/j.enconman.2015.07.082.

[50] D. Kramer, J. Zhang, R. Shimoi, E. Lehmann, A. Wokaun, K. Shinohara, G.G. Scherer, In situ diagnostic of two-phase flow phenomena in polymer electrolyte fuel cells by neutron imaging: Part A. Experimental, data treatment, and quantification, Electrochim. Acta. 50 (2005) 2603–2614. doi:10.1016/j.electacta.2004.11.005.

[51] Y.H. Park, J.A. Caton, Development of a PEM stack and performance analysis including the effects of water content in the membrane and cooling method, J. Power Sources. 179 (2008) 584–591. doi:10.1016/j.jpowsour.2008.01.050.

[52] K. Nishida, T. Murakami, S. Tsushima, S. Hirai, Measurement of liquid water content in cathode gas diffusion electrode of polymer electrolyte fuel cell, J. Power Sources. 195 (2010) 3365–3373. doi:10.1016/j.jpowsour.2009.12.073.

[53] L. You, H. Liu, A two-phase flow and transport model for the cathode of PEM fuel cells, Int. J. Heat Mass Transf. 45 (2002) 2277–2287. doi:10.1016/S0017-9310(01)00322-2.

[54] C. Song, Y. Tang, J.L. Zhang, J. Zhang, H. Wang, J. Shen, S. McDermid, J. Li, P. Kozak, PEM fuel cell reaction kinetics in the temperature range of 23-120 °C, Electrochim. Acta. 52 (2007) 2552–2561.

doi:10.1016/j.electacta.2006.09.008.

[55] C. Brunetto, A. Moschetto, G. Tina, PEM fuel cell testing by electrochemical impedance spectroscopy, Electr. Power Syst. Res. 79 (2009) 17–26. doi:10.1016/j.epsr.2008.05.012.

[56] P.M. Gomadam, J.W. Weidner, Analysis of electrochemical impedance spectroscopy in proton exchange membrane fuel cells, Int. J. Energy Res. 29 (2005) 1133–1151. doi:10.1002/er.1144.

[57] S. Asghari, A. Mokmeli, M. Samavati, Study of PEM fuel cell performance by electrochemical impedance spectroscopy, Int. J. Hydrogen Energy. 35 (2010) 9283–9290. doi:10.1016/j.ijhydene.2010.03.069.

[58] Y. Bultel, K. Wiezell, F. Jaouen, P. Ozil, G. Lindbergh, Investigation of mass transport in gas diffusion layer at the air cathode of a PEMFC, Electrochim. Acta. 51 (2005) 474–488. doi:10.1016/j.electacta.2005.05.007.

[59] I. Pivac, D. Bezmalinović, F. Barbir, Catalyst degradation diagnostics of proton exchange membrane fuel cells using electrochemical impedance spectroscopy, Int. J. Hydrogen Energy. 43 (2018) 13512–13520. doi:10.1016/j.ijhydene.2018.05.095.

[60] H.D. Ham, Influence of the water content on the kinetics of counter-ion transport in pefiuorosulphonic membranes, J. Electroanal. Chem. 287 (1998) 43–59. doi:10.1016/0022-0728(90)87159-H.

[61] Y. Wu, J.I.S. Cho, T.P. Neville, Q. Meyer, R. Zeische, P. Boillat, M. Cochet, P.R. Shearing, D.J.L. Brett, Effect of serpentine flow-field design on the water management of polymer electrolyte fuel cells: An in-operando neutron

radiography study, J. Power Sources. 399 (2018) 254–263. doi:10.1016/j.jpowsour.2018.07.085.

[62] Q. Yan, H. Toghiani, J. Wu, Investigation of water transport through membrane in a PEM fuel cell by water balance experiments, J. Power Sources. 158 (2006) 316–325. doi:10.1016/j.jpowsour.2005.09.013.

[63] T.J.P. Freire, E.R. Gonzalez, Effect of membrane characteristics and humidification conditions on the impedance response of polymer electrolyte fuel cells, J. Electroanal. Chem. 503 (2001) 57–68. doi:10.1016/S0022-0728(01)00364-3.

[64] P. Trogadas, V. Ramani, P. Strasser, T.F. Fuller, M.O. Coppens, Hierarchically Structured Nanomaterials for Electrochemical Energy Conversion, Angew. Chemie - Int. Ed. 55 (2016) 122–148. doi:10.1002/anie.201506394.

[65] F. Barbir, H. Gorgun, X. Wang, Relationship between pressure drop and cell resistance as a diagnostic tool for PEM fuel cells, J. Power Sources. 141 (2005) 96–101. doi:10.1016/j.jpowsour.2004.08.055.

[66] Y. Shao, L. Xu, J. Li, Z. Hu, C. Fang, J. Hu, D. Guo, M. Ouyang, Hysteresis of output voltage and liquid water transport in gas diffusion layer of polymer electrolyte fuel cells, Energy Convers. Manag. 185 (2019) 169–182. doi:10.1016/j.enconman.2019.01.084.

[67] J.R. Atkins, S.C. Savett, S.E. Creager, Large-scale current fluctuations in PEM fuel cells operating with reduced feed stream humidification, J. Power Sources. 128 (2004) 201–207. doi:10.1016/j.jpowsour.2003.09.067.

[68] N. Fouquet, C. Doulet, C. Nouillant, G. Dauphin-Tanguy, B. Ould-Bouamama,

Model based PEM fuel cell state-of-health monitoring via ac impedance measurements, J. Power Sources. 159 (2006) 905–913. doi:10.1016/j.jpowsour.2005.11.035.

[69] J.-M. Le Canut, R.M. Abouatallah, D.A. Harrington, Detection of Membrane Drying, Fuel Cell Flooding, and Anode Catalyst Poisoning on PEMFC Stacks by Electrochemical Impedance Spectroscopy, J. Electrochem. Soc. 153 (2006) A857. doi:10.1149/1.2179200.

[70] Y. Wang, L. Yue, S. Wang, New design of a cathode fl ow- fi eld with a sub-channel to improve the polymer electrolyte membrane fuel cell performance, J. Power Sources. 344 (2017) 32–38. doi:10.1016/j.jpowsour.2017.01.075.

[71] H. Li, Y. Tang, Z. Wang, Z. Shi, S. Wu, D. Song, J. Zhang, K. Fatih, J. Zhang, H. Wang, Z. Liu, R. Abouatallah, A. Mazza, A review of water flooding issues in the proton exchange membrane fuel cell, J. Power Sources.178 (2008) 103–117. doi:10.1016/j.jpowsour.2007.12.068.

[72] T.J. Mason, J. Millichamp, T.P. Neville, P.R. Shearing, S. Simons, D.J.L. Brett, A study of the effect of water management and electrode flooding on the dimensional change of polymer electrolyte fuel cells, J. Power Sources. 242 (2013) 70–77.J. Power Sources. 242 (2013) 70–77. doi:10.1016/j.jpowsour.2013.05.045.